5-2021

Analysis of Photodetector Based on Zinc Oxide and Cesium Lead Bromide Heterostructure with Interdigital Metallization

Tanveer Ahmed Siddique
University of Arkansas, Fayetteville

Analysis of Photodetector Based on Zinc Oxide and Cesium Lead Bromide Heterostructure with Interdigital Metallization

A thesis submitted in partial fulfilment
of the requirements for the degree of
Master of Science in Electrical Engineering

by

Tanveer Ahmed Siddique
Military Institute of Science and Technology
Bachelor of Science in Electrical, Electronics and Communication Engineering, 2016

May 2021
University of Arkansas

This thesis is approved for recommendation to the Graduate Council

Omar Manasreh, Ph.D.
Thesis Director

Samir M. El-Ghazaly, Ph.D.
Committee Member

Jeff Dix, Ph.D.
Committee Member

Bothina Manasreh, Ph.D.
Committee Member

ABSTRACT

In this thesis, photodetector based on the zinc oxide and cesium lead bromide hetero structure were fabricated and characterized. Zinc oxide (ZnO) nanoparticles were synthesized using solution processing and cesium lead bromide ($CsPbBr_3$) thin film was synthesized using two step deposition method. Three phonon modes were obtained by the Raman spectroscopy of ZnO nanoparticles. X-ray diffraction spectra of ZnO exhibits five exciton peaks which denotes that the synthesized ZnO structure was of good crystallinity with wurtzite hexagonal phase. The absorbance spectrum of ZnO shows the bandgap (E_g) in the order of 3.5 eV that aligns with reported results. The photoluminescence and the absorbance technique were used to measure the E_g of $CsPbBr_3$ in the order of 2.33 eV and 2.37 eV respectively which means the results are in good agreement. The current voltage (I-V) graph exhibits that due to the electron transfer from $CsPbBr_3$ to ZnO under illuminated light, the photocurrent was increased by a factor 2 greater than the dark current under the bias voltage of 6 V. Impulse time response of the photodetector was observed by measuring the current under light on and light off condition with an interval of 10 seconds. The photodetector was fabricated using the conventional wet etching lithography. Interdigital metallization structures were used with Au electrodes having 10μm gaps. The detectivity of the photodetector was measured to be 3.8×10^{11} cm / Hz^2 W from the I-V measurement. Under 10 μW light illumination the device showed good photo responsivity of 14.99 A/W. The fabricated photo detectors demonstrated excellent stability. This project explains that ZnO/$CsPbBr_3$ hetero structure is a promising candidate for high performance photodetector.

ACKNOWLEDGEMENTS

First of all, I would like to thank my thesis director and graduate advisor, Dr. Omar Manasreh for providing me the opportunity to work on this project. His supervision and constant support laid the foundation for my work on device fabrication and characterization. His direction and support helped me to complete this project. I am thankful to Dr. Samir M. El-Ghazaly, Dr. Jeff Dix and Dr. Bothina Manasreh for being in my thesis committee. I am also thankful to all my recent and current lab members for their support. I thank Dr. Mohammed Marie, Haider Salman and Amir Shariffar for their support which created an amazing research environment. My final thanks goes to my parents and my sister. Without their constant love and support it would have not been possible for me to finish my project.

TABLE OF CONTENTS

LIST OF FIGURES

LIST OF TABLES

1. INTRODUCTION

Organic and inorganic perovskite materials are receiving considerable attention in optoelectronic applications recently because of their unique physical properties. Perovskite materials exhibit long carrier diffusion lengths, high light absorption coefficients, long carrier lifetime and high carrier mobility [1], [2]. For these exceptional properties, photodetectors based on perovskite materials show excellent detectivity, responsivity and switching response [3], [4]. Lead halide perovskites, which is an inorganic perovskite material, $CsPbX_3$ (X = I, Br, Cl) showed less degradation and better stability in atmospheric conditions compared to organic perovskites [5]. Among the inorganic perovskites, cesium lead bromide ($CsPbBr_3$) has large carrier mobility (1000 cm^2/ Vs) and high absorption coefficient which are suitable for better performance of photodetectors [6]. However, hybrid inorganic-organic perovskites showed better performance then photodetectors based on single inorganic perovskite layer [6], [7]. By fabricating a hetero-structure of the perovskite layer with another material is one possible method to increase the performance of fabricated photodetectors. Due to high electron mobility, tunable conductivity, Zinc oxide (ZnO) is an encouraging material for the fabrication of hetero-structure perovskite photodetectors [7]. An effective design for high performance photodetector is interdigital metallization. Conventional photolithography technique is a better method to get interdigital metallization pattern on the device [8], [9]. This thesis will discuss about the fabrication process of ZnO nanoparticles and $CsPbBr_3$ thin film hetero-structure on photodetector with interdigital metallization for better performance.

1.1 Thesis overview

The motivation behind this thesis is to fabricate a photodetector that has hetero-structure of zinc oxide nanoparticles and perovskite material. Zinc oxide nanoparticles work as electron transport layer which increase the photocurrent and carrier recombination time. Due to that the device becomes faster and exhibits higher detectivity. In chapter one, the device structure and formation will be discussed. Chapter 2 discusses about the synthesis of materials and fabrication process of the photodetector device. Chapter 3 explains the characterization methods and modules used in this project. Chapter 4 analyses the characterized materials and the efficiency of the ZnO/$CsPbBr_3$ photodetector. This chapter also discusses the results and the effect of ZnO nanoparticles in the photodetector. Finally, chapter 5 concludes the thesis with the proposal of possible future work.

1.2 Zinc oxide nanoparticles as electron transport layer

In this thesis, we will see that after introducing the ZnO layer as an electron transport layer with $CsPbBr_3$, the responsivity, detectivity and switching speed of the fabricated photodetector increases compare to photodetector with only $CsPbBr_3$ photodetector. In the photodetector device with only $CsPbBr_3$, photo generated electron hole pair recombine in few picoseconds. It also depends on the life time of the photo excited electrons. Due to this reason, there is significant photocurrent loss. But, after introducing the ZnO nanoparticles layer as an electron transport layer, the photocurrent increases. The reason behind is the band alignment of the ZnO, perovskite and metal. The electron affinity of ZnO is 3.4 eV, electron affinity of perovskite ($CsPbBr_3$) is 4.4 eV and the work function of gold is 5 eV [10]. So, when light is incident on the device, photo excited electrons travel from perovskite to ZnO layer. And the holes in $CsPbBr_3$ moves to the metal. Due to the transfer of electrons from perovskite to ZnO,

the recombination process in the perovskite is very limited, which eventually increases the photocurrent. Zinc oxide has higher mobility so the electrons can move faster in the ZnO layer which is another reason of higher photocurrent [7].

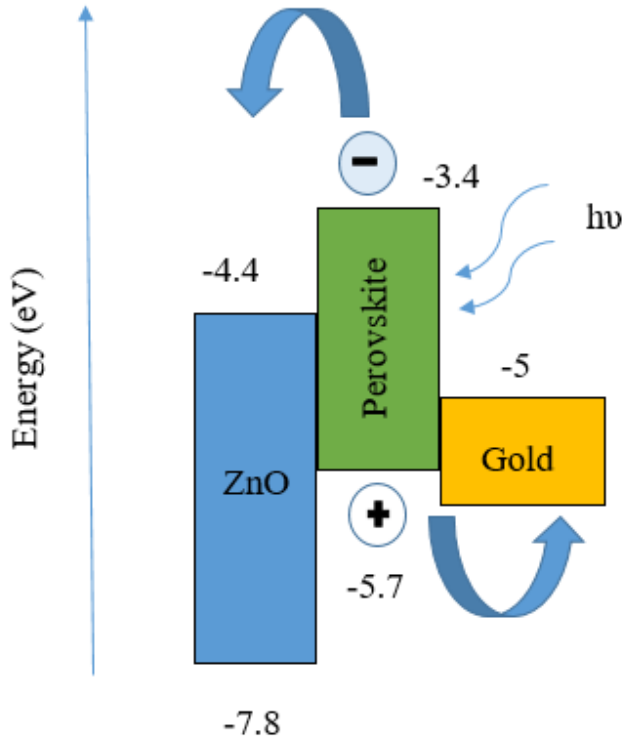

Figure. 1.1. The schematic is illustrating the electron transfer from perovskite to ZnO and hole transfer from perovskite to metal under light illumination.

1.3 Interdigital metallization

One of the challenges in hetero-structure photodetector is to maintain low dark current. Zinc oxide has good band alignment and stability with $CsPbBr_3$ [10]. For these reasons, ZnO and perovskite hetero-structure is used in perovskite solar cells and photodetectors [11], [12]. Interdigital metallization technique is an excellent design for photodetectors to maintain low dark current and high detectivity. Channel spacing of 10μm between two electrodes provides narrow

channels. The narrow channel allows the device to collect photo generated electron and holes before they get the chance to recombine. In several reported works, it is found that the reaction between metal and perovskite materials is one of the major reasons for the degradation of perovskite materials [13]. Copper, silver, gold and chromium electrodes are mostly used and there chemical reactions were investigated [13], [14]. Copper (Cu) electrodes are not very corrosive, but the direct contact between perovskite and Cu can create chemical reactions which might degrade the active perovskite material [13]. The high work function of Gold (Au) which is 5 eV, is most favorable with the fermi level of inorganic perovskite materials [14]. For this reason, Au electrodes were used for metallization to evaluate the performance of the device. Due to the work function of Au and the fermi level of $CsPbBr_3$, Au electrodes create a schottky barrier with ZnO/$CsPbBr_3$ hetero-structure. Due to good adhesion properties of glass and Au [15], the possibility of Au electrode getting removed during the depositions is very low.

1.4 Device structure

The fabricated device has a hetero structure of ZnO and $CsPbBr_3$. The substrate of the device was glass. First the glass substrates or the samples were cleaned. Then photolithography process was done to get the interdigital pattern. After that, metal was deposited on the patterned glass substrate to get the electrodes. When the device was fully patterned with electrodes, ZnO nanoparticles were deposited on the top of the fabricated device. On the top of the ZnO layer, $CsPbBr_3$ thin film was created to get the ZnO/$CsPbBr_3$ structure.

The fabrication process of $CsPbBr_3$ and ZnO photodetector is illustrated in the flow chart below:

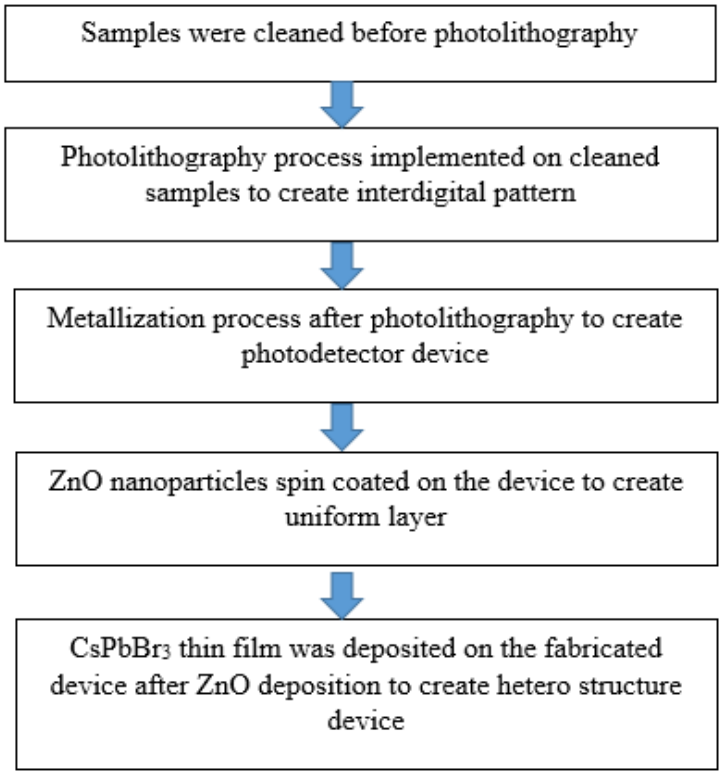

Figure. 1.2. A flowchart is shown to explain the step by step fabrication process of the ZnO/$CsPbBr_3$ device.

1.5 Working principle of ZnO/$CsPbBr_3$ photodetector

In this thesis, the optical characterization of ZnO nanoparticles and $CsPbBr_3$ thin films are reported and the applications ZnO/$CsPbBr_3$heterostructure in photodetectors are investigated. Perovskite materials have high absorption coefficient and larger carrier mobility which transports the photo induced electron hole pairs to the interface of $CsPbBr_3$/ZnO. Then due to the electric field, the electron hole pairs are separated thus creating photocurrent. The device here is fabricated using gold interdigital metallization for better performance. Figure 1.3

explains the working principle of the fabricated device. When light is incident on the device, the electron and hole pair are created. Due to the bandgap alignment, the electron moves to ZnO and the hole moves to perovskites. Thus the recombination in $CsPbBr_3$ is reduced and due this phenomenon, higher photocurrent can be observed. The absorption, Raman and photoluminescence spectra of the ZnO and $CsPbBr_3$ were measured to characterize. The devices were measured for higher photocurrent by using the I-V characteristic measurement. The time response of the photodetector was shown. In addition, the detectivity, responsivity and time response of the photodetector were measured from the I-V measurement.

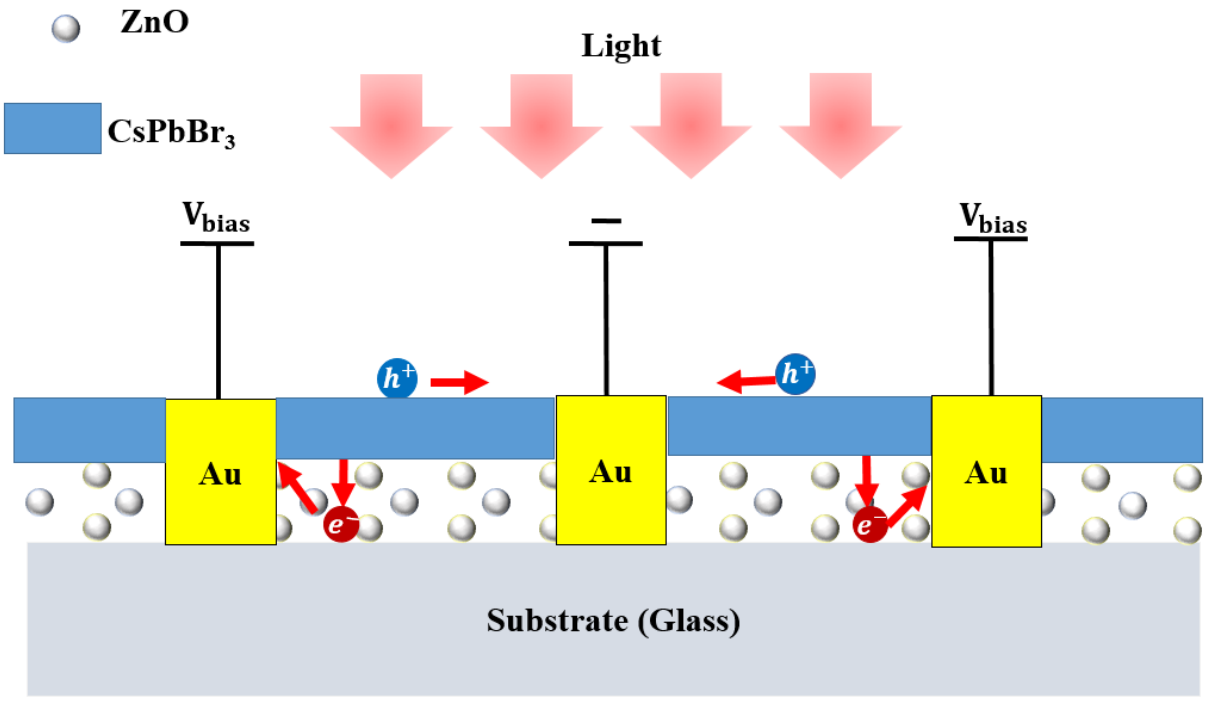

Figure. 1.3. The working principle of ZnO/$CsPbBr_3$ photodetector under light illumination is expressed by a simplified schematic.

2. SYNTHESIS OF MATERIALS AND DEVICE FABRICATION

2.1 Introduction

This chapter will briefly discuss about the synthesis process of ZnO nanoparticles and $CsPbBr_3$ thin film. This chapter will also discuss about all the procedures of device fabrication.

2.2 Synthesis of zinc oxide nanoparticles

Zinc oxide nanoparticles were used as an electron transport layer in the photodetector. For ZnO nanoparticles synthesis, 1.23g of zinc acetate di-hydrate was dissolved in 55ml of methanol and 0.48g of potassium hydroxide was dissolved in 25ml methanol. Then, potassium hydroxide solution was added dropwise in zinc acetate di-hydrate solution with magnetic stirring at 60^{o}C temperature and kept for 2 hours. After 2 hours, the product turned out to be a white precipitate which was washed with methanol. The purification process was done by centrifugation. Then nanoparticle were dried under N_2 vacuum to form powder. Finally, the dried nanoparticles of ZnO was dispersed in butanol (20mg / ml) for experimental use [16]. Figure 2.1 explains the whole process.

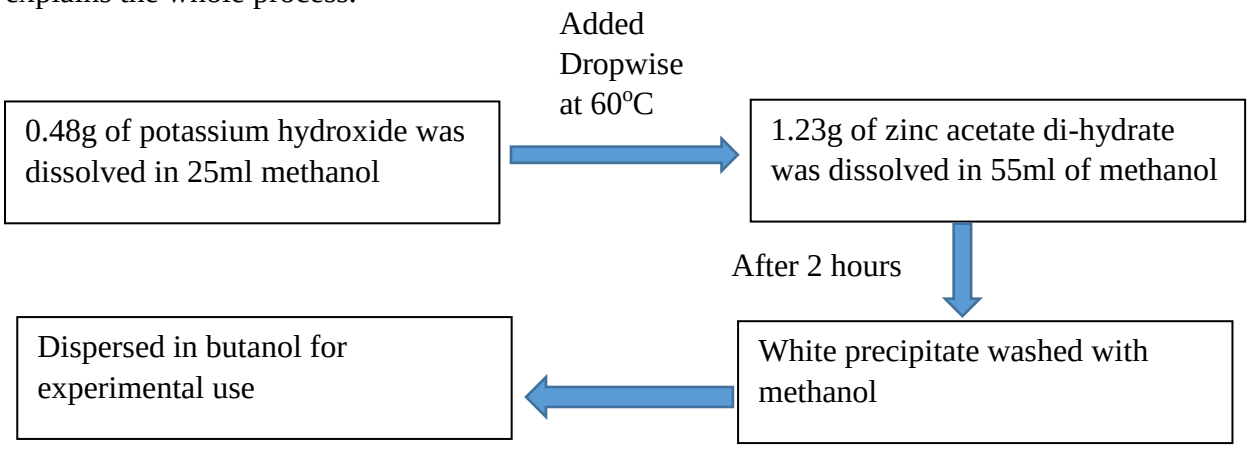

Figure. 2.1. Zinc Oxide nanoparticle synthesis process is illustrated through the flowchart.

Figure. 2.2. ZnO nanoparticles were smashed into powder form for measurement and characterization. “Photo by Tanveer Ahmed Siddique”

Figure. 2.3. ZnO nanoparticles were dispersed in Butanol for experimental use. “Photo by Tanveer Ahmed Siddique”

2.3 Synthesis of cesium lead bromide thin film

For the synthesis of cesium lead bromide ($CsPbBr_3$) thin film, two step deposition method was used [12]. 1 molar concentration of lead bromide ($PbBr_2$) in a mixture of dimethylformamide was kept 5 hours to form a clear solution. To create 1M $PbBr_2$, 367 mg of $PbBr_2$ merged in 10 ml of dimethylformamide. Then, 0.03M concentration of cesium

bromide (CsBr) in a mixture of methanol was created. To create this concentration, 30 mg of CsBr were dissolved in 2ml of methanol.

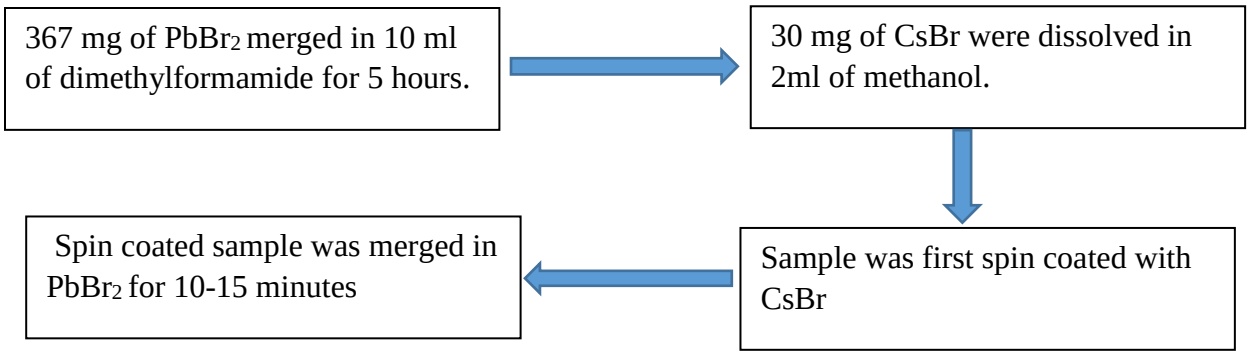

Figure 2.4. The step by step process of two step deposition method of $CsPbBr_3$ thin film is explained through the flowchart.

2.4 Fabrication of ZnO/$CsPbBr_3$ photodetector

The photodetector was fabricated in a class 100 clean room. Standard photolithography process was used to fabricate the device. The entire fabrication process can be divided into following major steps.

2.4.1 Sample cleaning

Acetone, methanol and isopropanol were used to clean the samples as these are strong organic solvents which remove impurities from the surface of the sample. First the samples were merged in acetone using ultra-sonication for 3 minutes. Then the samples were cleaned with de-ionized (DI) water and dried with N_2. After that, the cleaned samples were merged in methanol and ultra-sonication was used for 3 minutes. Then the samples were rinsed with DI water and dried with N_2. Same procedure was done with isopropanol. After these steps, samples were cleaned and ready to use.

2.4.2 Photolithography

The samples were patterned using positive photoresist and photomask in order to form 3mm X 3 mm mesas. The interdigital structure was used to patter the device. First, the cleaned samples were spin coated with AZ®P4330 positive photoresist with 3000 rpm for 60s. After completion of the spin coating, the samples were baked at 110^{o}C for 3 minutes. Then, the samples were carefully exposed to the UV light to create interdigital pattern of 10µm on the samples. After exposing to the UV light, the samples were developed in AZ® 400K developer for 45-50 seconds and then immediately dipped into DI water to stop the developing. After developing the pattern, the samples were loaded into the sample holder of the electron beam evaporator.

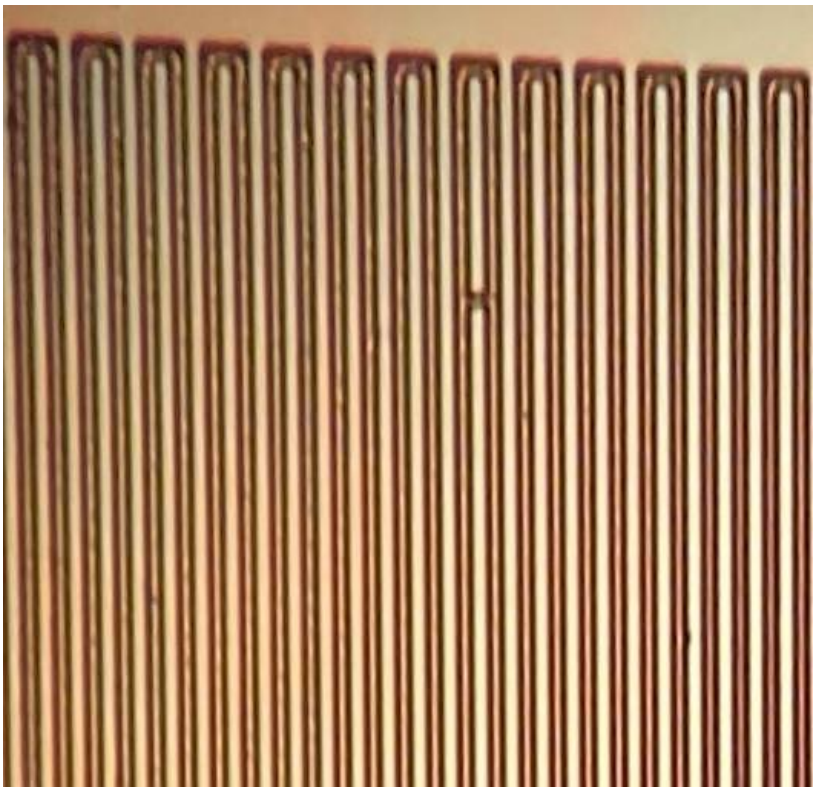

Figure 2.5. The microscopic view of the sample is showing the 10µm interdigital pattern on the samples after photolithography. “Photo by Tanveer Ahmed Siddique”

2.4.3 Metallization

To get the contact metals in the photodetector, the Angstrom Nexdep electron beam evaporator was used. Gold was deposited at the rate of 0.3nm/second. The total thickness of gold was 50 nm. The samples were heated a little during metallization process so that we can avoid the thermal stress which occurs because of rapid thermal annealing done to form ohmic contacts.

2.4.4 Lift off

After the metallization process, the samples were merged into acetone and kept in ultra-sonication to remove the excess metal. By this lift off process, the desired patter on the samples were created.

Figure 2.6. The microscopic view of the fabricated device is displaying 10µm interdigital pattern on the samples after lift-off process. “Photo by Tanveer Ahmed Siddique”

3. CHARACTERIZATION TECHNIQUES

3.1 Material characterization

This chapter describes the characterization techniques for synthesized materials. The absorbance spectra was measured using Cary 500 UV-Vis spectrophotometer. The Raman spectra and photoluminescence were measured using Horiba LabRam Micro-Raman spectrometer. The XRD measurement was taken by Rigaku Miniflex X-ray diffractometer. The current voltage characteristics of the fabricated device were measured with Keithley 4200 semiconductor characterization system.

3.1.1 Absorbance measurement

If light strikes on a semiconductor surface, photons with higher energy than the semiconductor band gap gets absorbed. Incident photons with lower energy than the bandgap gets transmitted. The Uv-Vis spectrophotometer measures the absorbance and transmittance. In the project, this device is used to measure the absorbance of ZnO nanoparticles and $CsPbBr_3$ thin film. The bandgap of the materials were observed from the absorbance spectra. The peak of the absorbance spectra of these materials indicated the approximate band gap of the material. From the Beer-Lambert law, the following equation was used to calculate the absorbance [12],

$$I = I_o e^{-\alpha d} \tag{3.1}$$

Where, I is the intensity of transmitted light through the material, I_o is the incident light. α is the absorbance coefficient and d is the optical path length of the material. The spectrometer can measure wavelength range of 175 nm – 3300 nm.

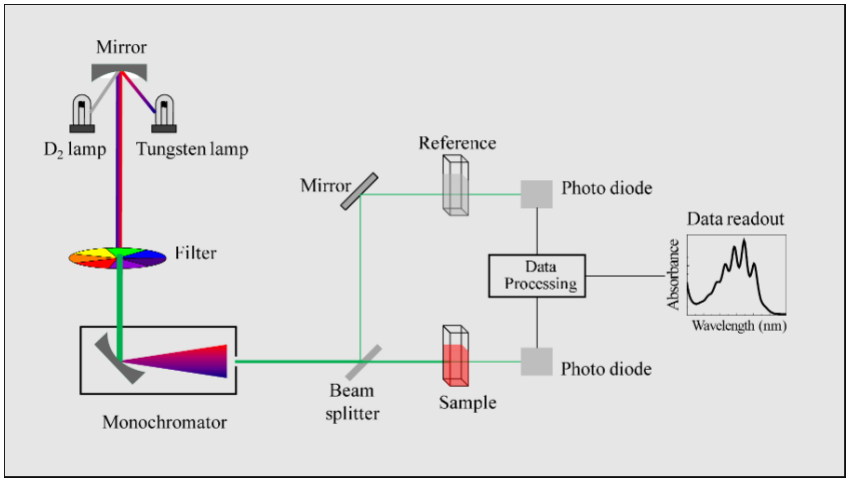

(a)

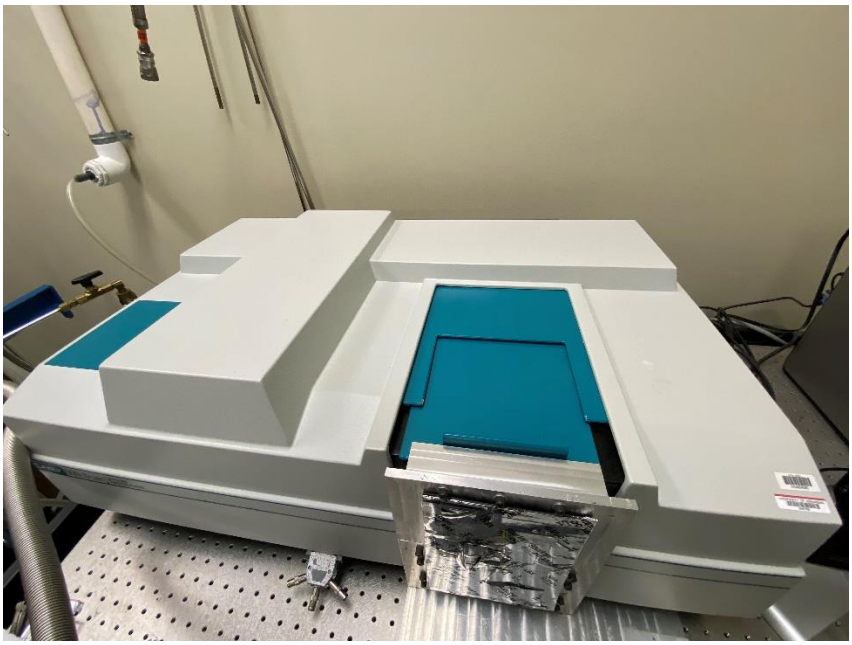

(b)

Figure 3.1. (a) The schematic explains the working principle of the absorbance spectroscopy [18]. (b) A photo of Cary 500 UV-Vis spectrophotometer situated in the lab. “Photo by Tanveer Ahmed Siddique”

3.1.2 Raman spectroscopy

Raman spectroscopy is a common characterization method which provides information of structural properties of a material. The structural orientation, chemical composition, crystallinity of a material is characterized through Raman spectroscopy. Inelastic Raman scattering process and phonon vibration mechanism are showed the Figure 3.2. By using the concept of electronic states, the Stokes and anti-Stokes are explained in the energy diagram. The Raman shift is plotted verses the intensity. Raman spectroscopy gives information regarding the molecular structure in the material, the orientation of the molecules and chemical composition. The scattered radiation from the molecules of the sample provides sufficient information about the energy increase or decrease. From this vibrational energy, Raman shift is measured. In this project, the Raman spectroscopy was used to characterized ZnO nanoparticles and the fabricated device by using Horiba LabRAM Micro-Raman spectomter.

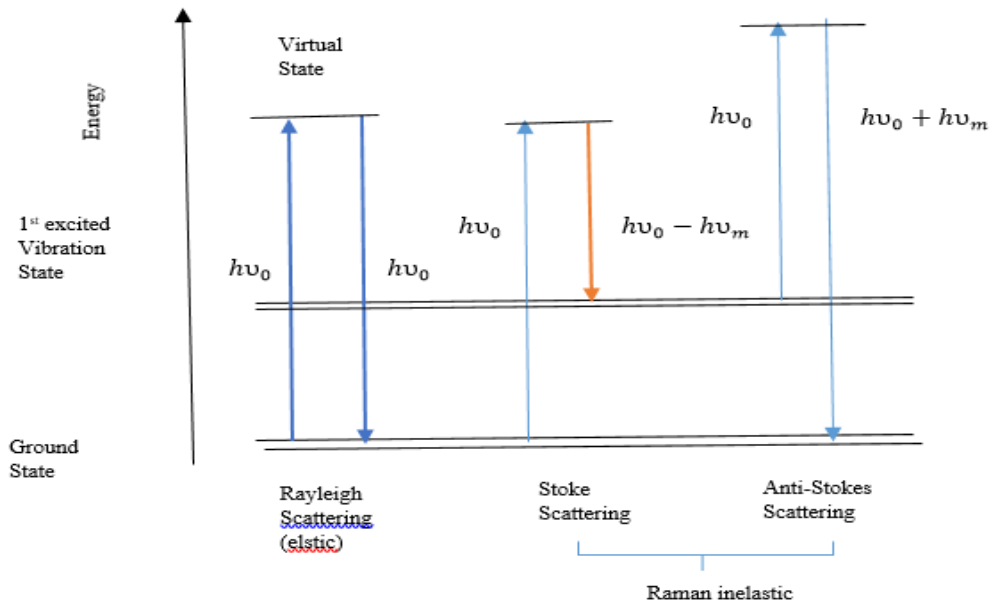

Figure 3.2. The schematic diagram of the energy bands are shown to explain the Raman scattering.

3.1.3 Luminescence

When laser is incident on semiconductor, the excited carriers forms radiative recombination of excitons. This is known as luminescence. To produce considerable luminescence, the radiative recombination must dominate non-radiative recombination. Non-equilibrium carrier concentration is produced by optical excitation and it is called photoluminescence. All the materials used in this project was characterized through the photoluminescence. By changing the filters in Horiba LabRAM Micro-Raman spectrometer, photoluminescence characterization method was used. By using the photoluminescence method, approximate bandgap were measured from the excitation peak of the synthesized materials.

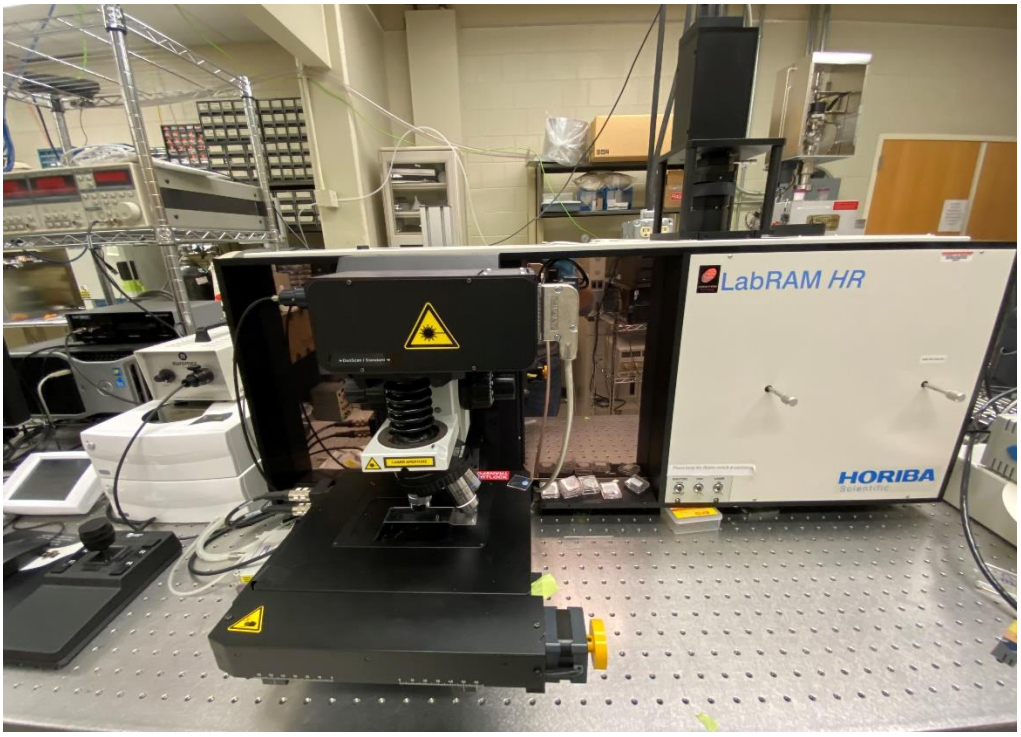

Figure 3.3. Horiba LabRAM Micro-Raman spectrometer located in the lab was used to characterize the materials. “Photo by Tanveer Ahmed Siddique”

3.1.4 X-ray diffraction

X-ray Diffraction (XRD) is a known characterization technique to get information about the crystallinity of the materials. In a crystal, atoms are organized in lattice in different patterns. The length between two lattice points is known as the lattice constant. There are different planes in the crystal structure and when x-ray is incident on any crystal structure, they scatter elastically from different planes in crystal which is known as Thompson scattering. And the scattered electron oscillates as the same frequency as the incident x-ray. The x-ray beams are scattered differently in plays from which different diffraction pattern. By analyzing the diffraction spacing and pattern, the crystal structure gets defined. Bragg's law is the pattern analyzing equation to determine the crystal structure. The equation is given below.

$$2d\sin\theta = n\lambda \tag{3.2}$$

Where, d is the distance or length between lattice planes, n is an integer, θ is the scattering angle and λ is the wavelength. In Figure 3.4, the Bragg's law is explained properly.

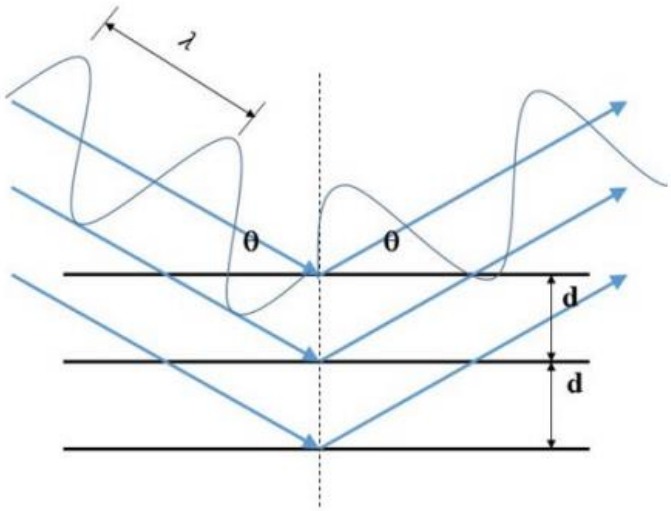

Figure 3.4. The schematic is representing the working principle of X-ray based on the mechanism of Bragg's law [26].

In lab, Rigaku Miniflex X-ray diffractometer is used to get the XRD patterns for ZnO nanoparticles and $CsPbBr_3$ thin film.

Figure 3.5. Rigaku Miniflex X-ray diffractometer was used to measure the XRD patters of the synthesized materials. “Photo by Tanveer Ahmed Siddique”

3.2 Device characterization

This section briefly discusses about the characterization techniques for the fabricated device. A Keithley 4200 semiconductor characterization module was used for measuring the I-V characteristics curves using 0.2 sun to 1 sun AM 1.5 solar simulator.

3.2.1 I-V characteristics measurement

Keithley 4200 semiconductor characterization system was used to measure the I-V characteristics curves of fabricated photodetector. The system is equipped with two source measure units (SMU). In this project, I-V characteristics curve of the fabricated devices with ZnO/$CsPbBr_3$ and $CsPbBr_3$ materials were measured. Built-in 2-wire forward bias diode test module was used to take the measurements. The anode voltage was swept from -6 V to 6 V. Photocurrent and dark current were measured. The impulse response of the photodetector was measured with Keithley 4200 semiconductor characterization system.

4. RESULTS AND DISCUSSION

4.1 Introduction

This chapter briefly discusses about the obtained results from synthesized materials and fabricated device. The Raman and XRD confirms about the pristine ZnO nanoparticles quality. The Photoluminescence and absorbance of both ZnO nanoparticles and $CsPbBr_3$ thin films are in good agreement with the reported results. The I-V characteristics curve proves that fabricated photodetector with ZnO/$CsPbBr_3$ has higher detectivity and photo response compare to photodetector with $CsPbBr_3$.

4.1.1 Device fabrication

To fabricate the device, first glass samples were cleaned thoroughly. Then photolithography and metallization process was done to create interdigitated pattern. After that, first ZnO nanoparticles were deposited on the interdigitated substrate and was annealed at 100^0C for 30 minutes. Then, lead bromide was spin coated on the substrate with ZnO and was annealed at 90^0C for 30 minutes. After that the device was merged in cesium bromide for 5 – 15 minutes

at 50^0C to form the heterostucture device. The device was kept on 180^0C for 10 minutes to remove all solvents.

4.1.2 Zinc oxide nanoparticles characterization

The absorbance spectra of ZnO nanoparticles are shown in figure. 4.1. Synthesized nanoparticles of ZnO were dispersed in butanol (20 mg/ml). The red line in the figure represents the absorbance of ZnO nanoparticles dispersed in butanol. The peak was observed at 350 nm. The band gap calculated from the peak is 3.5 eV form 350 nm. The nanoparticle dispersed in butanol showed a bit higher bandgap with less wider peak. The reason behind is the size of the nanoparticle.

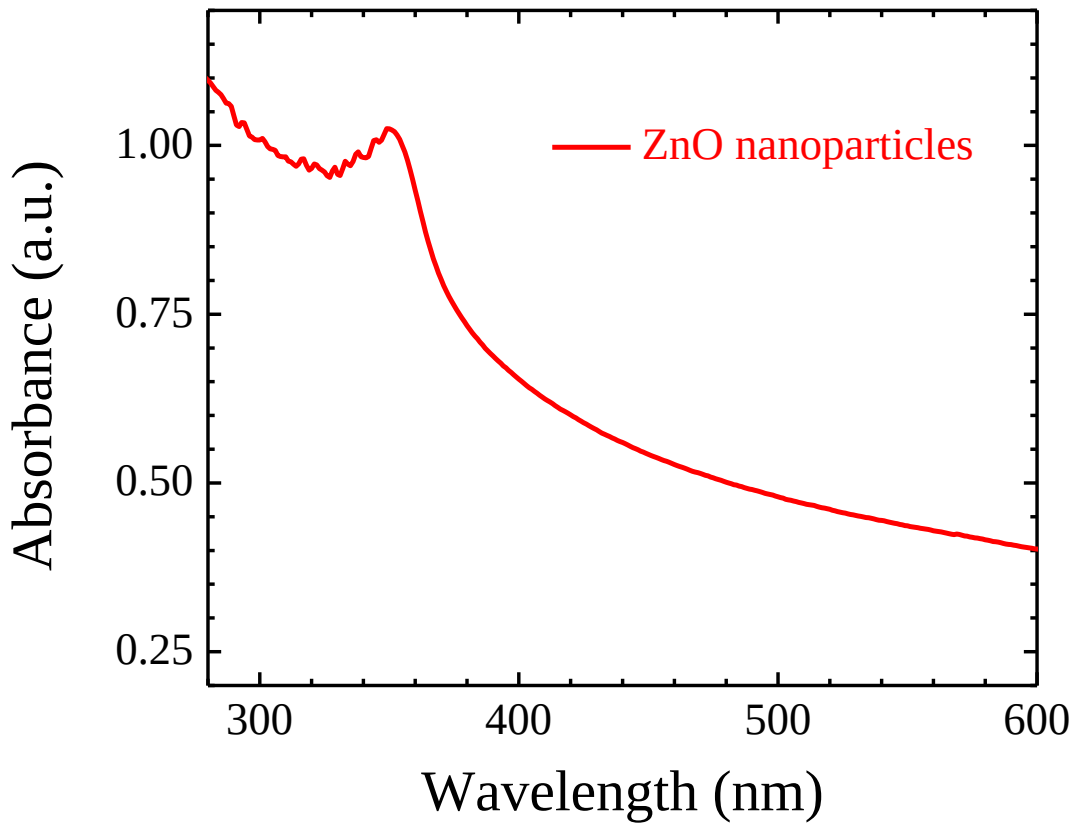

Figure. 4.1. The absorbance of ZnO nanoparticles was measured as a function of wavelength.

The Raman spectra of ZnO nanoparticles are shown in figure 4.2 with 632 nm laser light as an excitation source. ZnO has wurtzite crystal structure and ZnO has eight sets of optical phonon modes according to the group theory. The sharp and dominant peak was observed at 445 nm which is labeled as E_{2H}. E_{2H} is the higher frequency of the E_2 optical phonon mode and this mode is characteristic of wurtzite hexagonal phase of ZnO nanoparticles. E_2 optical phonon modes has to peak usually known as E_{2L} phonon mode which is found in lower frequency and E_{2H} phonon mode found at higher frequency.

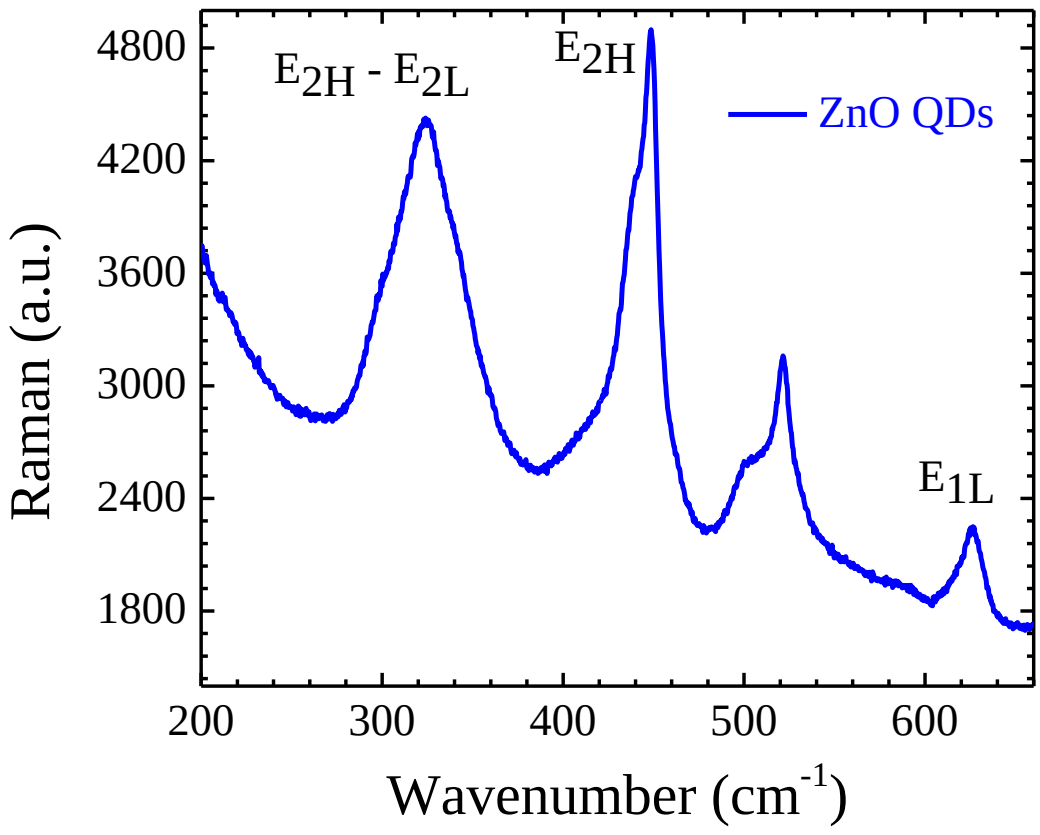

Figure. 4.2. The Raman spectroscopy of ZnO nanoparticles was measured as a function of wavenumber.

Other phonon modes are also observed at 330 nm and 615 nm which is labeled in the figure as $E_{2H} - E_{2L}$ and E_{1L}. But the dominant peak at 445 nm compared to other peaks demonstrates that synthesized ZnO structure was of good crystallinity with wurtzite hexagonal phase [10].

Figure 4.3 shows five XRD peaks of ZnO nanoparticles. The angles at 26.3^{O}, 34.4^{O}, 54^{O}, 59.8^{O} and at 70^{O}. At high intensity of X-ray, planes (hkl) for the ZnO are (100) at 26.3^{O}, (101) at 34.4^{O}, (110) at 54^{O}, (103) at 59.8^{O} and (201) at 70^{O}. The peaks demonstrates that synthesized ZnO structure was of good crystallinity with wurtzite hexagonal phase [10].

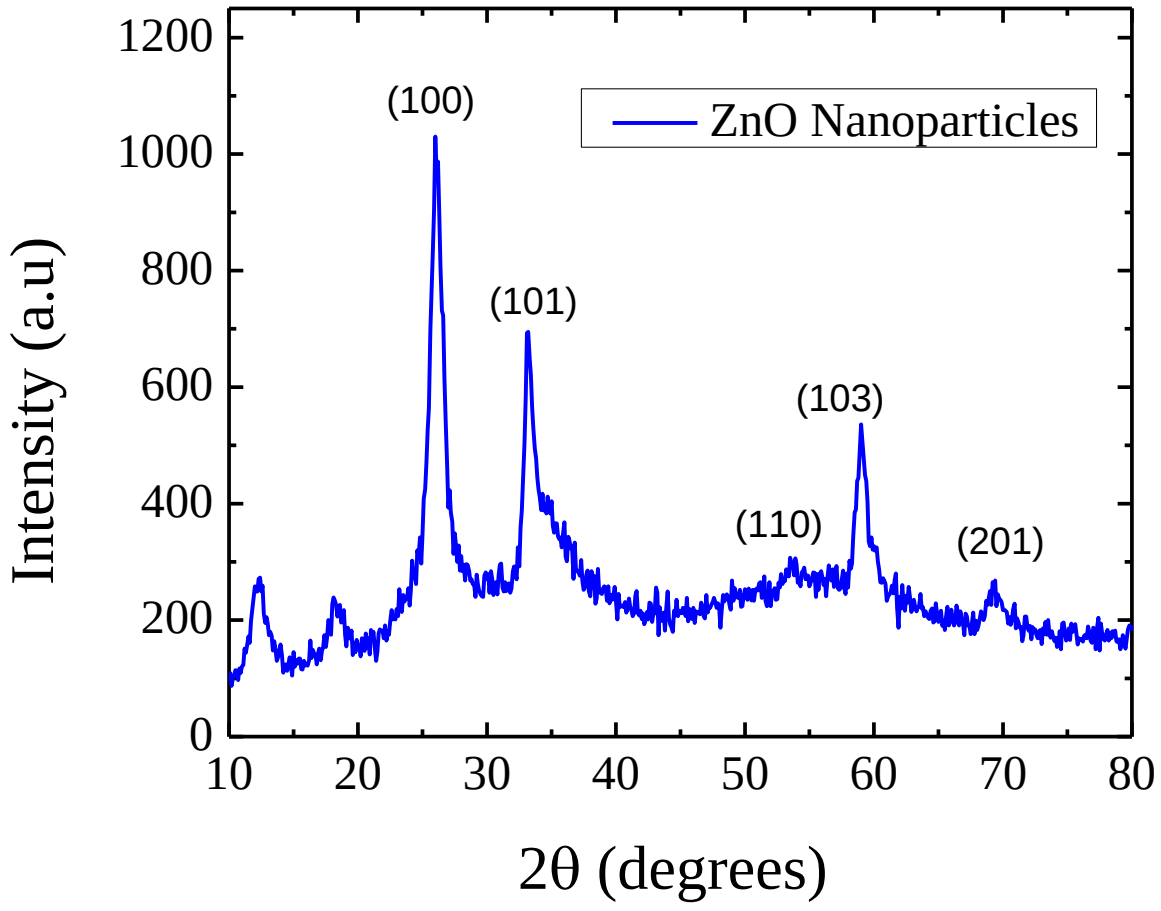

Figure. 4.3. The XRD pattern of ZnO nanoparticles as a function of angle validates the crystallinity of ZnO.

4.1.3 Cesium lead bromide thin film characterization

Cesium lead bromide ($CsPbBr_3$) thin film was synthesized on a glass substrate to characterize. The absorbance spectra and the photoluminescence spectra of $CsPbBr_3$ thin film on glass substrate are shown in figure 4.4. The peak in the photoluminescence spectra was observed at 530nm. The bandgap of $CsPbBr_3$ was calculated to be 2.33 eV from the photoluminescence spectra. The peak was observed at 522 nm in the absorbance spectra and the bandgap was calculated to be 2.37 eV from the peak and it is in good agreement with the literatures [12].

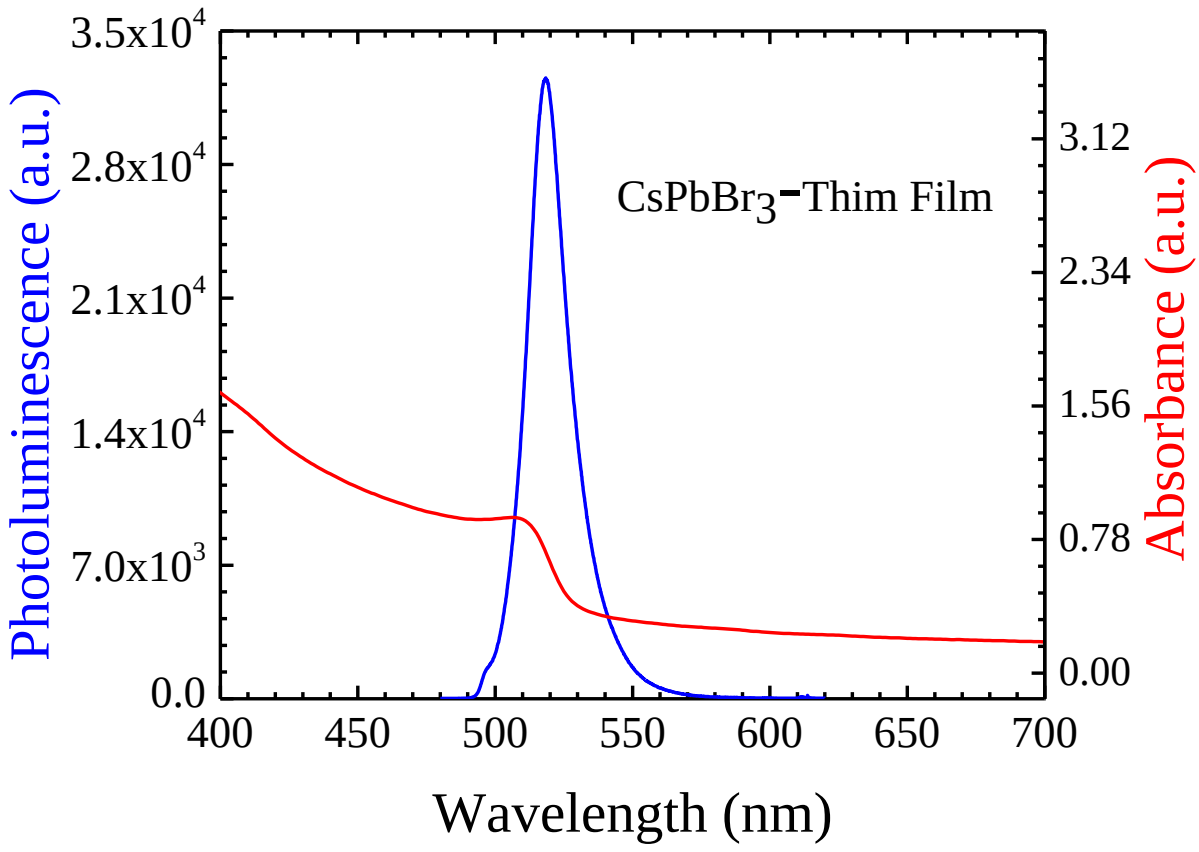

Figure. 4.4. The photoluminescence and the absorbance of $CsPbBr_3$ thin film were measured as a function of wavelength.

The wavelength of the blue laser used in the measurement was 472 nm and the intensity was 12 nW which is very low. It indicates that at low laser power, the $CsPbBr_3$ thin film generates high carrier density. Which means that the synthesized $CsPbBr_3$ thin film is good quality material.

Figure 4.5 shows four XRD peaks of CsPbBr3 thin film. The peaks at 23^O, 32.4^O, 38^O and 45.8^O proves that synthesized CsPbBr3 thin film structure was of good crystallinity with orthorhombic phase [17].

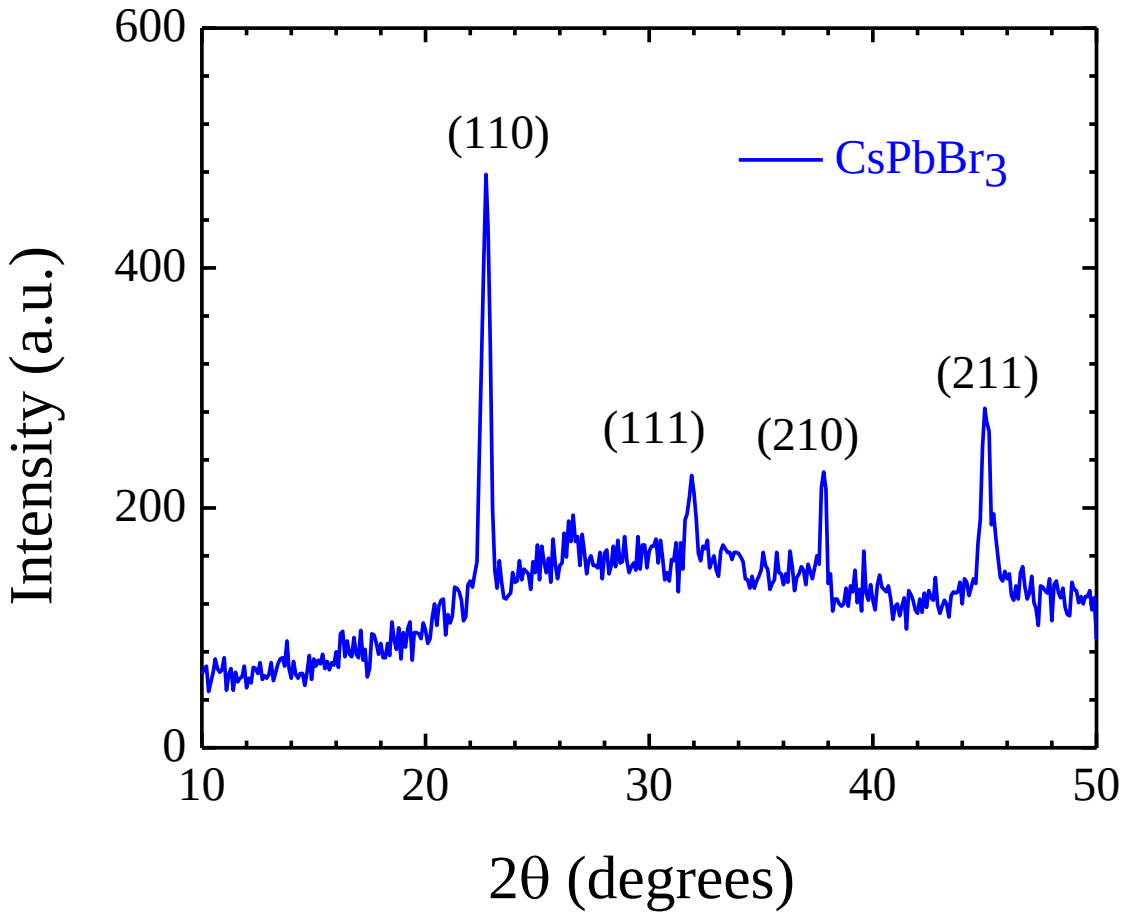

Figure. 4.5. The measured XRD pattern of $CsPbBr_3$ thin film as a function of angle was used to validate the crystallinity of $CsPbBr_3$.

4.2 Characterization of the fabricated device

Figure 4.6 shows the absorbance of ZnO/$CsPbBr_3$ as a function of wavelength. The absorbance is identical with the absorbance of $CsPbBr_3$. The reason behind is the top layer of the fabricated device is the perovskite. And due to that reason the incoming light is absorbed by the perovskite. The absorbance spectra of ZnO/$CsPbBr_3$ exhibits peak intensity at 515 nm.

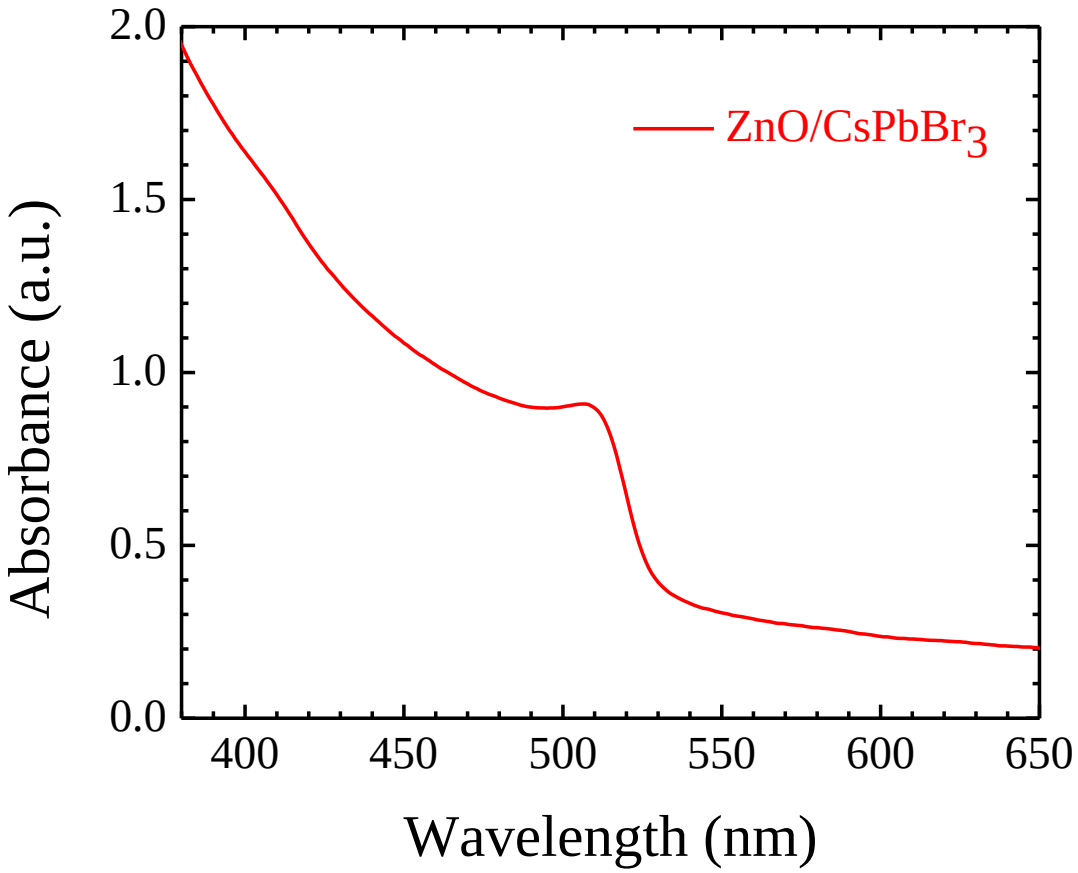

Figure. 4.6 The measured absorbance spectra of ZnO/$CsPbBr_3$ as a function of wavelength validates the presence of ZnO.

Figure 4.7 is the photoluminescence spectra of $CsPbBr_3$ thin film and ZnO/$CsPbBr_3$ as a function of wavelength. The maximum photoluminescence intensity of the fabricated device is

518 nm. From the figure, it is clear that the photoluminescence intensity is low for the fabricated device. ZnO layer reduces the recombination of the generated electron hole pair. So, when light illuminates on the device, the recombination is less for $ZnO/CsPbBr_3$ compare to $CsPbBr_3$. And the photoluminescence depends of the radiative recombination of generated electron and hole. So, due to the presence of ZnO layer, the photoluminescence intensity is lower for the fabricated device. There is also a small shift in photoluminescence for the fabricated device that is due the presence of ZnO layer.

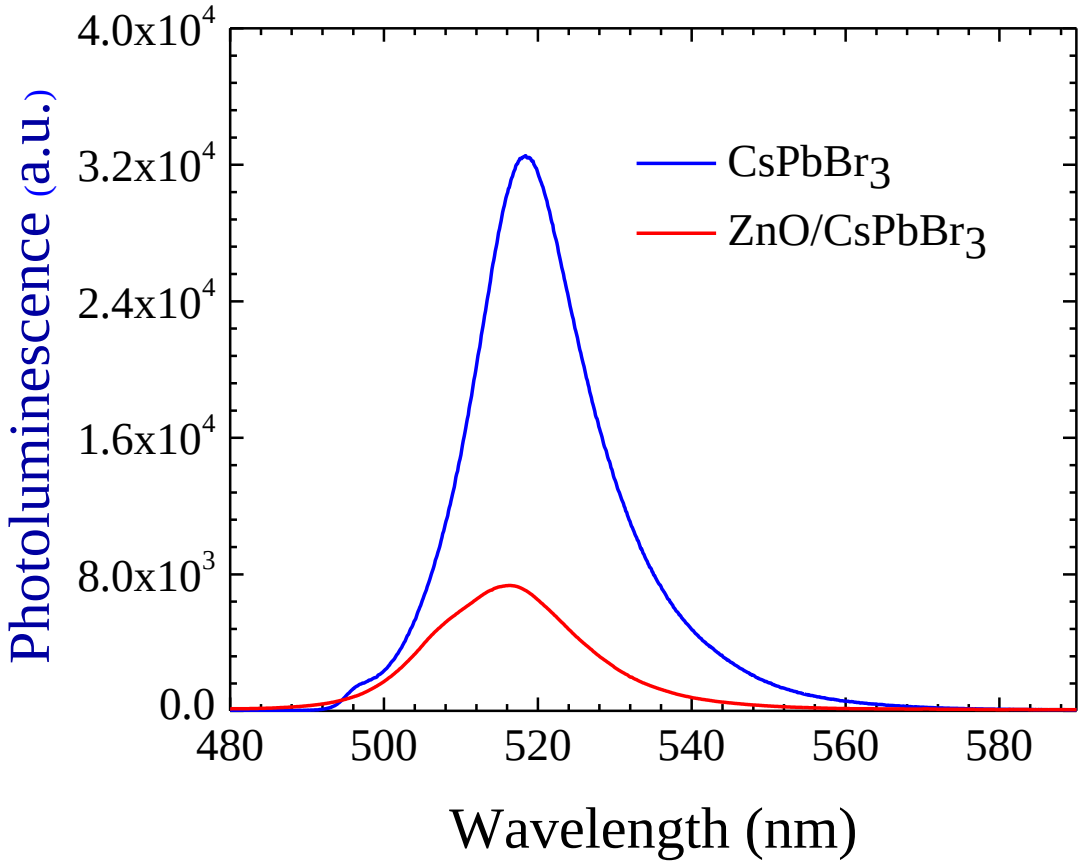

Figure. 4.7 The photoluminescence spectra of $CsPbBr_3$ thin film and $ZnO/CsPbBr_3$ as a function of wavelength were measured.

4.3 ZnO/$CsPbBr_3$ based photodetector I-V measurements and discussion

The I-V curve of the fabricated device is shown in Fig. 4.5 with sweeping voltage from 6V to -6V under dark and light condition. From the figure it is observed that the photocurrent of the device was enhanced by a factor of 2 greater than the dark current. Due to the unique optical properties of $CsPbBr_3$ and ZnO, the incident light produces excess amount of electron hole pair at 6V bias voltage. Due to this reason the photo current was higher in ZnO/$CsPbBr_3$ photodetector than $CsPbBr_3$ photodetector.

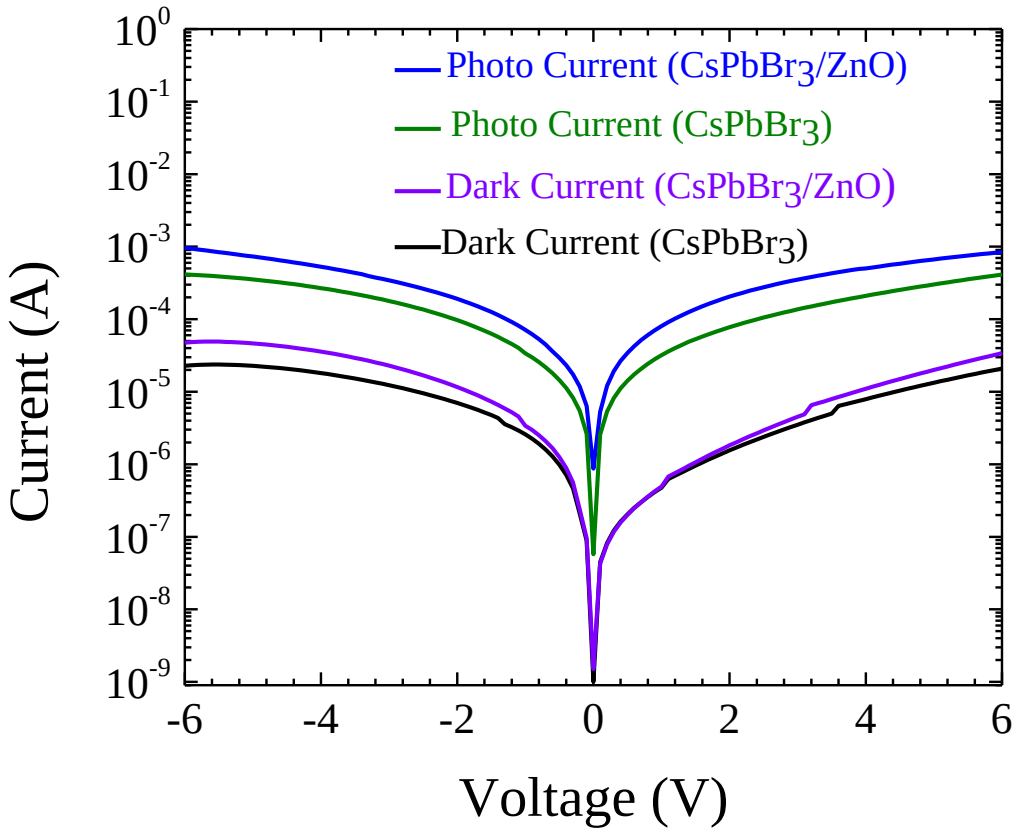

Figure. 4.8. The I-V curve of both $CsPbBr_3$ and fabricated photodetectors were measured under dark and light conditions.

In figure 4.8, the blue and black lines represents I-V curve of the ZnO/$CsPbBr_3$ photodetector under illuminated light condition and dark condition respectively. The green and violet line denotes the I-V curve of the $CsPbBr_3$ photodetector under illuminated light condition and dark condition respectively. The dark current with ZnO is higher than the dark current without ZnO. The reason behind this is due to the band tilt of the semiconductors and metals. When we change the polarity the band tilts, and thus there is difference between the 6V and -6V bias voltage.

To understand the effect of ZnO layer introduced in the fabricated device, the optical properties of ZnO/$CsPbBr_3$ and $CsPbBr_3$ devices were investigated. I-V curve shown in figure 4.5 represents the photo current and dark current of both ZnO/$CsPbBr_3$ and $CsPbBr_3$ photodetectors. It can be seen that the photocurrent of the ZnO/$CsPbBr_3$ device was enhanced by a factor of 2 greater than the dark current whereas photocurrent of the CsPbBr3 device was enhanced by a factor of 1.5 greater than the dark current. The detectivity and responsivity of the both photodetectors were measured from the I-V curve. The following equations are for detectivity and responsivity [21, 25]

$$D^* = \frac{I_{Ph}\sqrt{A}}{P\sqrt{2qI_d}} \tag{4.1}$$

$$R = \frac{I_{ph}}{P \times A} \tag{4.2}$$

In equation (4.1), D^* is the detectivity given in cm/Hz^2 W, A is the area of photodetector, P is the power of incident light, I_{Ph} and I_d are photo and dark current respectively, q is the electron charge. The incident power of the light was swept from 10 μW cm^{-2} to 100 mW cm^{-2}, at 100 mW cm^{-2} photo current and dark current were measured 10^{-3} A and 10^{-5} A respectively for ZnO/$CsPbBr_3$ photodetector. So from the equation the detectivity was measured. The measured

detectivity was 3.8×10^{11} cm / Hz^2 W at 100 mW cm^{-2}. For 10 μW cm^{-2}, measured detectivity was 5.25×10^{12} cm / Hz^2 W. For $CsPbBr_3$, photo current and dark current were measured 3×10^{-4} A and 8×10^{-5} A respectively at 100 mW cm^{-2}. From which the detectivity was measured 5.7×10^{10} cm / Hz^2 W. It can be inferred that in presence of the ZnO nanoparticles, the photo excited electrons in the perovskite moved to ZnO layer. Due to that the reason photocurrent is higher in ZnO/$CsPbBr_3$ photodetector [7-9], [16]. ZnO also has higher mobility compared to perovskite, so the photocurrent is higher in ZnO/$CsPbBr_3$ photodetector and has higher detectivity and responsivity. Reported works show that the detectivity of photodetectors based on $CsPbBr_3$ thin films are about 3.6×10^{11} cm / Hz^2 W [2-5], [17]. So, by introducing ZnO layer, the detectivity was increased due to higher photocurrent.

In equation (4.2), R is the responsivity, A is the area of photodetector, P is the power of incident light, I_{Ph} is photo current. The incident power of the light was swept from 10 μW cm^{-2} to 100 mW cm^{-2}, at 100 mW cm^{-2} incident power intensity, the responsivity was 0.09 (A/W). But at 10 μW, the responsivity was around 14.99 (A/W).

Table 4.1. The detectivity and the responsivity of fabricated $CsPbBr_3$ and ZnO/$CsPbBr_3$ photodetectors are compared based on different power intensity.

Power Intensity (mW cm^{-2})	Detectivity (cm / Hz^2 W)		Responsivity (A/W)	
	$CsPbBr_3$	ZnO/$CsPbBr_3$	$CsPbBr_3$	ZnO/$CsPbBr_3$
0.01	7.1×10^{11}	5.25×10^{12}	6.24	14.99
20	6.41×10^{10}	4.5×10^{11}	0.06	0.072
40	6.26×10^{10}	4.25×10^{11}	0.051	0.061
60	6.16×10^{10}	4×10^{11}	0.044	0.0612
80	5.9×10^{10}	3.92×10^{11}	0.045	0.063
100	5.7×10^{10}	3.8×10^{11}	0.039	0.09

From the table 4.1, it is evident that by introducing the ZnO layer, the detectivity and the responsivity of the fabricated device were increased.

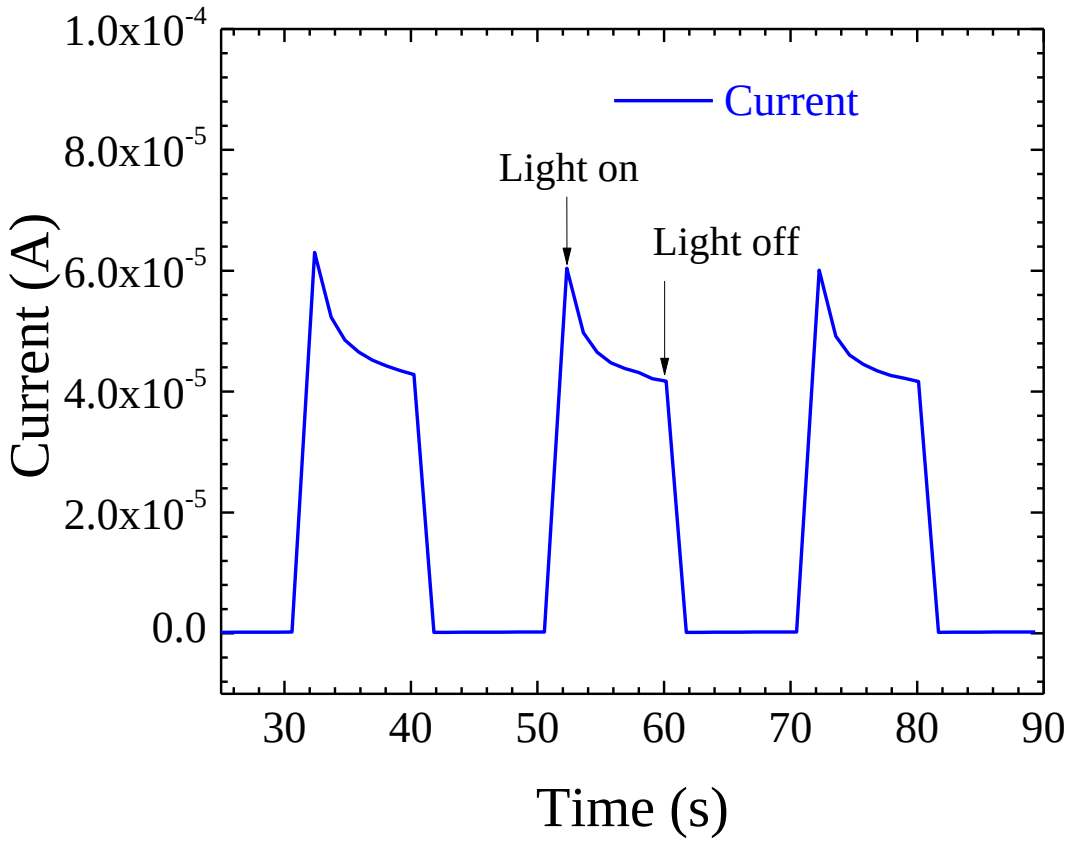

Figure. 4.9. The current of ZnO/$CsPbBr_3$ photodetector was calculated as a function of time under light on and light off condition with an interval of 10 seconds to compute switching response of the device.

The time response of the photodetector was observed and investigated in figure 4.9 by switching on and off the light source at 5V bias voltage. The current of the photodetector was measured as a function of time. Current was measured under light on and light off condition with an interval of 10 seconds. The rise time was 0.3 seconds and the fall time was 0.5 seconds. The time response was measured under light simulator with 100 $mWcm^{-2}$ power intensity.

In figure 4.9, there are some spikes in between on and off interval of ZnO/$CsPbBr_3$ photodetector. The spikes are due to the high rate of generated photo excited electrons and carrier drift velocity [21], [22]. The intensity of the light source used in this experiment was one sun which covers the spectral range from 300 to 1800 nm. Other reported works show that the rise time and fall time for $CsPbBr_3$ based photodetectors are 0.4 seconds and 0.5 seconds respectively [22-24], [25].

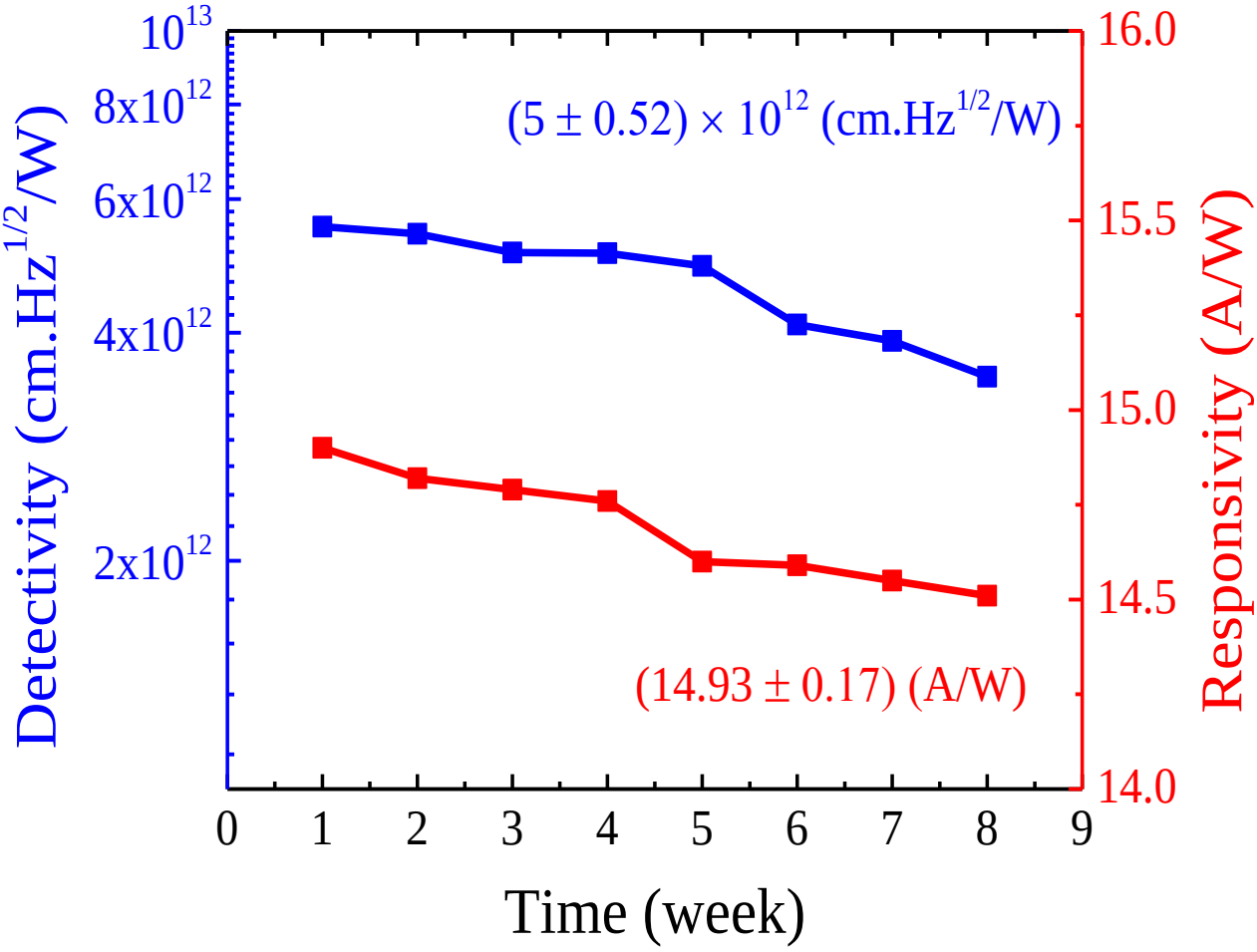

Figure. 4.10. The detectivity and responsivity data of the fabricated ZnO/$CsPbBr_3$ photodetector over time was taken to observe the stability of the device.

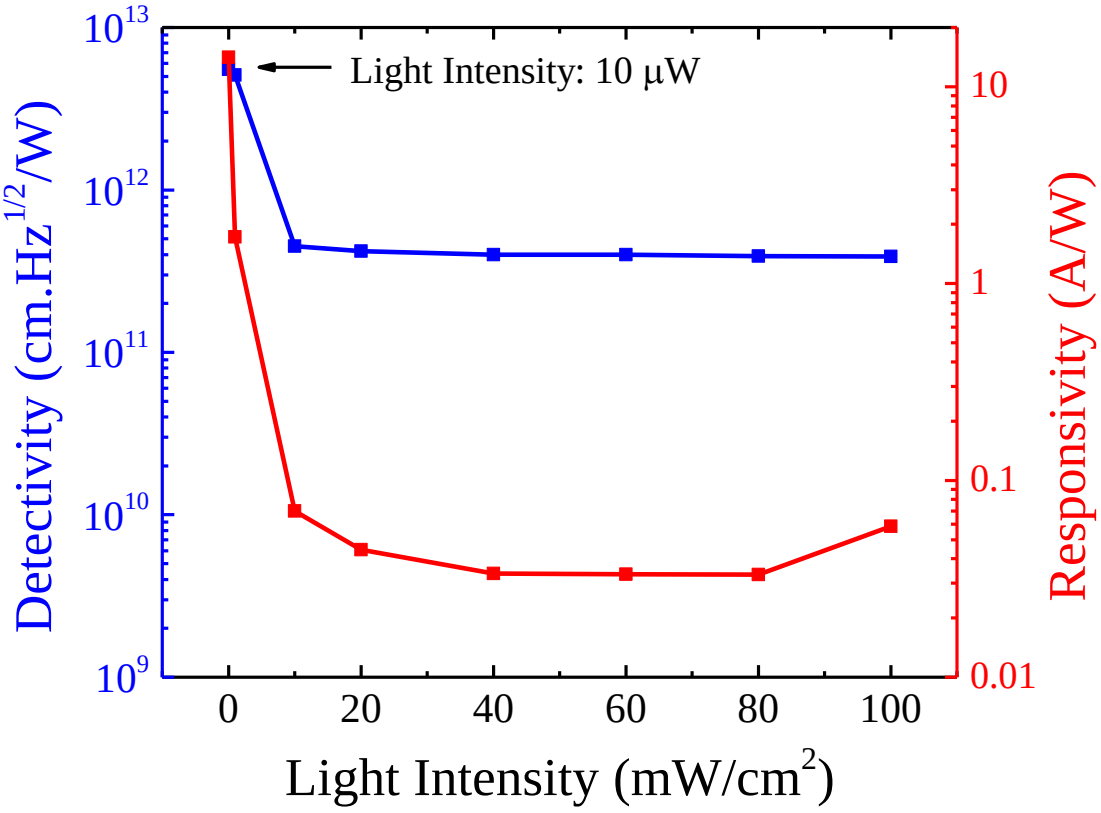

Figure. 4.11. The detectivity and responsivity of the fabricated device were measured as a function of light intensity.

Figure. 4.10 and Figure. 4.11 shows the detectivity and responsivity of the fabricated device. The detectivity of the photodetector was measured to be 5.25×10^{12} cm / Hz^2 W from the I-V measurement. Under 10 μW light illumination the device showed good photo responsivity of 14.99 A/W. The fabricated photo detectors demonstrated excellent stability compare to other devices fabricated with organic perovskite. The detectivity is usually stable for 3 to 4 weeks for organic perovskite photodetectors [23-26]. From the measurements of $ZnO/CsPbBr_3$ photodetector, it can be seen that the rise time and fall time are less which means that the fabricated device was faster. Higher and stable detectivity and faster switching speed was observed in $ZnO/CsPbBr_3$ photodetector due to the introduction of ZnO layer.

Table. 4.2. The responsivity and the rise/fall time of ZnO/$CsPbBr_3$ photodetector are compared with reported works on perovskite photodetectors.

Device Pattern	Material	Responsivity (A/W)	Rise/Fall time (s)	Ref
Cr/ $CsPbBr_3$/Cr	Thin film	0.2	0.7/0.9	[2]
Carbon/$CsPbBr_3$/FTO	Thin film	0.127	0.2/0.2	[27]
Ag/ $CsPbBr_3$/ITO	Nanowire	11.2	<3/<2	[28]
Ag/$CsPbBr_3$/Ag	Nanocrystal	1.8	1.8/1.2	[29]
Au/ZnO- $CsPbBr_3$/Au	Thin film	14.99	0.3/0.5	This work

From table 4.2, it is evident that by using ZnO layer with $CsPbBr_3$, the responsivity was higher than reported single layer $CsPbBr_3$ photodetectors. The rise and the fall time of the fabricated device is better than most of the reported $CsPbBr_3$ photodetector.

5. CONCLUSION AND FUTURE WORK

5.1 Conclusion

In conclusion, photodetectors based on the ZnO/ $CsPbBr_3$ hetero structure were investigated and characterized. ZnO nanoparticles were synthesized using solution process and the $CsPbBr_3$ was synthesized using two step deposition method. The ZnO layer worked as an electron transport layer in the device. Owing to the unique optical properties of $CsPbBr_3$ thin film and ZnO nanoparticles as electron transport layer, the photocurrent was enhanced after introducing ZnO layer in the $CsPbBr_3$ photodetector. The results obtained in this project indicate that ZnO/$CsPbBr_3$ hetero structure photodetectors exhibit excellent detectivity, responsivity and faster time response due to the electron transfer from $CsPbBr_3$ to the ZnO layer. The bandgap of both materials measured from the absorbance and photoluminescence are all in good agreements. The Raman spectra and XRD of the synthesized nanoparticle proved that ZnO nanoparticles were in wurtzite hexagonal phase. The fabricated photodetector's detectivity and

responsivity graphs explained that the devices were stable and shows high detectivity. The presented work shows that by introducing ZnO layer in $CsPbBr_3$ photodetector with interdigital metallization increases the photocurrent. The detectivity was also enhanced along with higher responsivity. These results indicate that photodetectors based on ZnO/$CsPbBr_3$ hetero structure fabricated with solution processing method show great potential in optical applications.

5.2 Future work

In this project, ZnO nanoparticles were used as an electron transport layer along with $CsPbBr_3$ thin films which enhanced the photocurrent. The structure showed better performance and stability. The ZnO layer can be exchanged with other n type material such as titanium oxide (TiO_2). This structure might work and might show better results in detectivity and responsivity. In that case, the bandgap of the material should be compatible with the perovskite material. The perovskite material can also be changed with halides or mixed halides (I, Cl etc.). In that case, we have to keep in mind about the stability of the mixed halide perovskite with the deposited n type layer. By replacing organic perovskite with inorganic perovskite might give better result. The metal used as anode and cathode can be replaced with chromium while using organic perovskite. Also, ZnO nanorods can be a promising candidate along with the organic perovskite materials for high performance photodetector.

REFERENCES

[1] Yu-Che Hsiao, Ting Wu, Mingxing Li, Qing Liu, Wei Qin and Bin Hu, "Fundamental physics behind high-efficiency organo-metal halide perovskite solar cells," *J. Mater. Chem. A*, vol. 3, no. 30, pp. 15372–15385, 2015, doi.org/10.1039/C5TA01376C.

[2] Haider Salman, Amir Shariffar, Tanveer Siddique, Wafaa Gebril, Andrian V Kuchuk, and M Omar Manasreh, "$CsPbBr_3$ perovskite photodetector with interdigital chromium electrodes," *Eng. Res. Express*, Oct. 2020, doi.org/10.1088/2631-8695/abbf90.

[3] S. D. Stranks, G. E. Eperon, G. Grancini, C. Menelaou, M. J. P. Alcocer, T. Leijtens, L. M. Herz, A. Petrozza, H. J. Snaith, "Electron-Hole Diffusion Lengths Exceeding 1 Micrometer in an Organometal Trihalide Perovskite Absorber, " *Science*, vol. 342, no. 6156, pp. 341–344, Oct. 2013, doi.org/10.1126/science.1243982.

[4] G. Xing, N. Mathews, S. Sun, S. S. Lim, Y. M. Lam, M. Gratzel, S. Mhaisalkar, T. C. Sum, "Long-Range Balanced Electron and Hole-Transport Lengths in Organic-Inorganic CH3NH3PbI3," *Science*, vol. 342, no. 6156, pp. 344–347, Oct. 2013, doi.org/10.1126/science.1243167.

[5] Letian Dou, Yang (Micheal) Yang, Jingbi You, Ziruo Hong, Wei-Hsuan Chang, Gang Li, Yang Yang "Solution-processed hybrid perovskite photodetectors with high detectivity," *Nat Commun*, vol. 5, no. 1, p. 5404, Dec. 2014, doi.org/10.1038/ncomms6404.

[6] Gurivi Reddy Yettapu, Debnath Talukdar, Sohini Sarkar, Abhishek Swarnkar, Angshuman Nag, Prasenjit Ghosh, Pankaj Mandal, "Terahertz Conductivity within Colloidal $CsPbBr_3$ Perovskite Nanocrystals: Remarkably High Carrier Mobilities and Large Diffusion Lengths," *Nano Lett.*, vol. 16, no. 8, pp. 4838–4848, Aug. 2016, doi.org/10.1021/acs.nanolett.6b01168.

[7] Yang Ma, Congjun Wu, Zhihao Xu, Fei Wang and Min Wang, "Separating light absorption layer from channel in ZnO vertical nanorod arrays based photodetectors for high-performance image sensors," *Appl. Phys. Lett.* vol. 112, no. 19, p. 191103, May 2018, doi.org/10.1063/1.5011645.

[8] Wen-jia Zhou, Kui-juan Jin, Hai-zhong Guo, Chen Ge, Meng He and Hui-bin Lu, "Electrode effect on high-detectivity ultraviolet photodetectors based on perovskite oxides," *Journal of Applied Physics*, vol. 114, no. 22, p. 224503, Dec. 2013, doi.org/10.1063/1.4845775.

[9] Jie Xue, Yu Gu, Qingsong Shan, Yousheng Zou, Jizhong Song, Leimeng Xu, Yuhui Dong, Jianhai Li, Haibo Zeng, "Constructing Mie-Scattering Porous Interface-Fused Perovskite Films to Synergistically Boost Light Harvesting and Carrier Transport," *Angew. Chem. Int. Ed.*, vol. 56, no. 19, pp. 5232–5236, May 2017, doi.org/10.1002/anie.201700600.

[10] Feng Teng, Lingxi a Zheng, Kai Hu, Hongyu Chen, Yanmei Li, Zhiming Zhang, Xiaosheng Fang, " A surface oxide thin layer of copper nanowires enhanced the UV selective response of a ZnO film photodetector, " J. Mater. Chem. C, vol. 4, No. 36, pp. 8416 – 8421, 2016, doi.org/10.1039/C6TC02901A.

[11] Mulmudi Hemant Kumar, Natalia Yantara, Sabba Dharani, Michael Graetzel, Subodh Mhaisalkar, Pablo P. Boix, Nripan Mathews, "Flexible, low-temperature, solution processed ZnO-based perovskite solid state solar cells," Chem. Common., vol. 49, no. 94, p. 11089, 2013, doi.org/10.1039/c3cc46534a.

[12] Dianyi Liu and Timothy L. Kelly, "Perovskite solar cells with a planar heterojunction structure prepared using room-temperature solution processing Techniques," *Nature Photon*, vol. 8, no. 2, pp. 133–138, Feb. 2014, doi.org/10.1038/nphoton.2013.342.

[13] F. Behrouznejad, S. Shahbazi, N. Taghavinia, Hui-Ping Wu and Eric Wei-Guang Diau, "A study on utilizing different metals as the back contact of $CH_3NH_3PbI_3$ perovskite solar cells," *J. Mater. Chem. A*, vol. 4, no. 35, pp. 13488–13498, 2016, doi.org/10.1039/C6TA05938D.

[14] Konrad Domanski, Juan-Pablo Correa-Baena, Nicolas Mine, Mohammad Khaja Nazeeruddin, Antonio Abate, Michael Saliba, Wolfgang Tress, Anders Hagfeldt, Michael Grätzel, "Not All That Glitters Is Gold: Metal-Migration-Induced Degradation in Perovskite Solar Cells," ACS *Nano*, vol. 10, no. 6, pp. 6306–6314, Jun. 2016, doi.org/10.1021/acsnano.6b02613.

[15] Jingjing Zhao, Xiaopeng Zheng, Yehao Deng, Tao Li, Yuchuan Shao, Alexei Gruverman, Jeffrey Shield, Jinsong Huang, "Is Cu a stable electrode material in hybrid perovskite solar cells for a 30-year lifetime?," *Energy Environ. Sci.*, vol. 9, No. 12, pp. 3650–3656, 2016, doi.org/10.1039/C6EE02980A.

[16] Eric Moyen, Joo Hyun Kim, Jeonggi Kim and Jin Jang, "ZnO Nanoparticles for Quantum – Dot - Based Light – Emitting Diodes," *ACS Appl. Nano Mater.*, vol. 3, no. 6, pp. 5203 – 5211, Jun. 2020, doi.org/10.1021/acsanm.0c00639.

[17] Ying Li, Zhi-Feng Shi, Sen Li, Ling-Zhi Lei, Hui-Fang Ji, Di Wu, Ting-Ting Xu, Yong – Tao Tian, Xin-Jian Li, "High-performance perovskite photodetectors based on Solution-processed all-inorganic $CsPbBr_3$ thin films," J. Mater. Chem. C, vol. 5, no. 33, pp. 8355–8360, 2017, doi.org/10.1039/C7TC02137B

[18] Andy Baker and Robert G.M. Spencer, "Characterization of dissolved organic matter from source to sea using fluorescence and absorbance spectroscopy," Science of The Total Environment, vol. 333, no. 1–3, pp. 217–232, Oct. 2004, doi.org/10.1016/j.scitotenv.2004.04.013.

[19] Wei Tian, Huanping Zhou, and Liang Li, "Hybrid Organic-Inorganic Perovskite Photodetectors," *Small*, vol. 13, no. 41, p. 1702107, Nov. 2017 doi.org/10.1002/smll.201702107 .

[20] Dong Li, Guifang Dong, Wenzhe Li, and Liduo Wang, "High performance organic-inorganic perovskite-optocoupler based on low-voltage and fast response perovskite compound photodetector," *Sci Rep*, vol. 5, no. 1, p. 7902, Jul. 2015, doi.org/10.1038/srep07902.

[21] Chenglong Li, Hailu Wang, Fang Wang, Tengfei Li "Ultrafast and broadband photodetectors based on a perovskite/organic bulk heterojunction for large-dynamic-range imaging," *Light Sci Appl*, vol. 9, no. 1, p. 31, Dec.2020, doi.org/10.1038/s41377-020-0264-5.

[22] Mahshid Ahmadi, Ting Wu, and Bin Hu, "A Review on Organic-Inorganic Halide Perovskite Photodetectors: Device Engineering and Fundamental Physics," *Adv. Mater.*, vol. 29, no. 41, p. 1605242, Nov. 2017, doi.org/10.1002/adma.201605242.

[23] Guoqing Tong, Maowei Jiang, Dae-Yong Son, Longbin Qiu, Zonghao Liu, Luis K. Ono, Yabing Qi, "Inverse Growth of Large-Grain-Size and Stable Inorganic Perovskite Micronanowire Photodetectors," *ACS Appl. Mater. Interfaces*, vol. 12, no. 12, pp. 14185–14194, Mar. 2020, doi.org/10.1021/acsami.0c01056.

[24] Parthiban Ramasamy, Da-Hye Lim, Bumjin Kim, Seung-Ho Lee, Min-Sang Lee, and Jong-Soo Lee, "All-inorganic cesium lead halide perovskite nanocrystals for photodetector applications," *Chem. Commun.*, vol. 52, no. 10, pp. 2067–2070, 2016, doi.org/10.1039/C5CC08643D.

[25] Cunlong Li, Ceng Han, Yubo Zhang, Zhigang Zang, Ming Wang, Xiaosheng Tang, Jihe Du "Enhanced photoresponse of self-powered perovskite photodetector based on ZnO nanoparticles decorated $CsPbBr_3$ films," *Solar Energy Materials and Solar Cells*, vol. 172, pp. 341–346, Dec. 2017, doi.org/10.1016/j.solmat.2017.08.014.

[26] Xiang Wang, Sheng-Chao Huang, Shu Hu, Sen Yan, and Bin Ren, "Fundamental understanding and applications of plasmon-enhanced Raman spectroscopy," *Nat Rev Phys*, vol. 2, no. 5, pp. 253–271, May 2020, doi.org/10.1038/s42254-020-0171-y.

[27] Ronghuan Liu, Jianqiang Zhang, Hai Zhou, Zehao Song, Zhaoning Song, Corey R. Grice, Dingjun Wu, Liangping Shen, Hao Wang, “Solution-Processed High-Quality Cesium Lead Bromine Perovskite Photodetectors with High Detectivity for Application in Visible Light Communication,” Adv. Optical Mater., vol. 8, no. 8, p. 1901735, Apr. 2020, doi.10.1002/adom.201901735.

[28] Shikai Yan, Qing Li, Xu Zhang, Sheng Tang, Wei Lei, and Jing Chen, “A vertical structure photodetector based on all-inorganic perovskite quantum dots,” *J Soc Inf Display*, vol. 28, no. 1, pp. 9–15, Jan. 2020, doi: 10.1002/jsid.853. doi.org/10.1002/jsid.853.

[29] Shuai Ye, Minghuai Yu, Wei Yan, Jun Song, and Junle Qu, “Enhanced photoluminescence of $CsPbBr_3$ @Ag hybrid perovskite quantum dots,” *J. Mater. Chem. C*, vol. 5, no. 32, pp. 8187–8193, 2017, doi: 10.1039/C7TC01969F.